Article

Structure

Structure of the MORN4/Myo3a Tail Complex Reveals MORN Repeats as Protein Binding Modules

Graphical Abstract

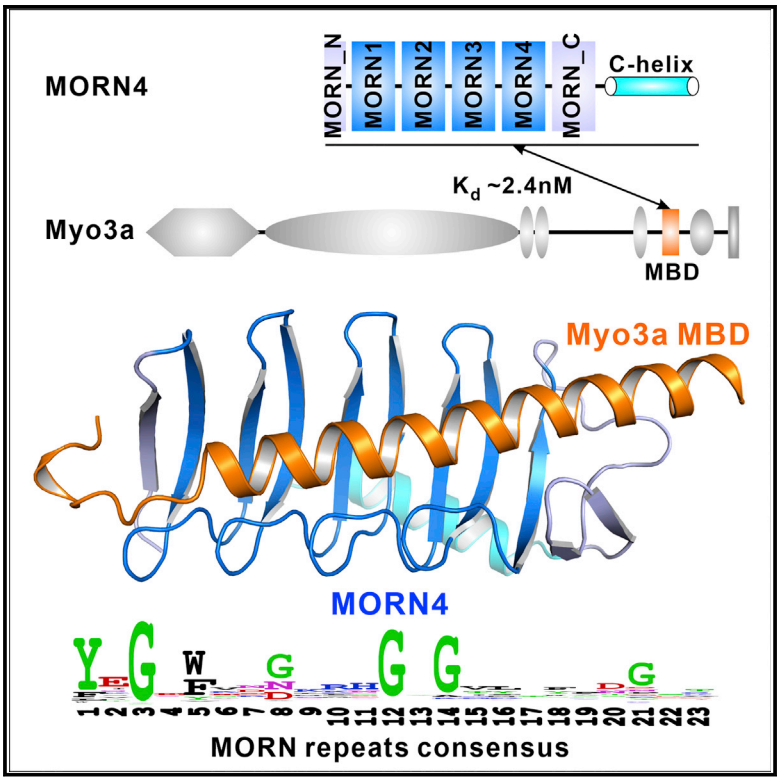

Highlights

- MORN4 binds to Myo3a tail with a very high affinity
- MORN4 forms a single-layered β sheet and binds to a long helix of Myo3a
- MORN4 filopodial tip localization depends on its binding to Myo3a
- MORN repeats are versatile protein-protein interaction modules

Authors

Jianchao Li, Haiyang Liu, Manmeet H. Raval, Jun Wan, Christopher M. Yengo, Wei Liu, Mingjie Zhang

Correspondence

liuwei@sphmc.org (W.L.), mzhang@ust.hk (M.Z.)

In Brief

The crystal structure of MORN4/Myo3a complex reveals that MORN4 can use its highly conserved U-shaped groove to interact with Myo3a tail with high affinity and specificity and suggests that MORN repeats are versatile protein-protein interaction modules.

Data Resources

6JLE

Li et al., 2019, Structure *27*, 1–9
September 3, 2019
https://doi.org/10.1016/j.str.2019.06.004

CellPress

Please cite this article in press as: Li et al., Structure of the MORN4/Myo3a Tail Complex Reveals MORN Repeats as Protein Binding Modules, Structure (2019), https://doi.org/10.1016/j.str.2019.06.004

Structure
Article

Structure of the MORN4/Myo3a Tail Complex Reveals MORN Repeats as Protein Binding Modules

Jianchao Li,[1,4,6] Haiyang Liu,[1,2,6] Manmeet H. Raval,[3,7] Jun Wan,[1,2] Christopher M. Yengo,[3] Wei Liu,[2,*] and Mingjie Zhang[1,2,5,8,*]

[1]Division of Life Science, State Key Laboratory of Molecular Neuroscience, Hong Kong University of Science and Technology, Clear Water Bay, Kowloon, Hong Kong, China
[2]Shenzhen Key Laboratory for Neuronal Structural Biology, Biomedical Research Institute, Shenzhen Peking University-The Hong Kong University of Science and Technology Medical Center, Shenzhen 518036, China
[3]Department of Cellular and Molecular Physiology, Pennsylvania State University College of Medicine, Hershey, PA 17033, USA
[4]Division of Cell, Developmental and Integrative Biology, School of Medicine, South China University of Technology, Guangzhou 510006, China
[5]Center of Systems Biology and Human Health, School of Science and Institute for Advanced Study, Hong Kong University of Science and Technology, Clear Water Bay, Kowloon, Hong Kong, China
[6]These authors contributed equally
[7]Present address: Eli and Edythe Broad CIRM Center for Regenerative Medicine and Stem Cell Research, University of Southern California, Los Angeles, CA 90033, USA
[8]Lead Contact
*Correspondence: liuwei@sphmc.org (W.L.), mzhang@ust.hk (M.Z.)
https://doi.org/10.1016/j.str.2019.06.004

SUMMARY

Tandem repeats are basic building blocks for constructing proteins with diverse structures and functions. Compared with extensively studied α-helix-based tandem repeats such as ankyrin, tetratricopeptide, armadillo, and HEAT repeat proteins, relatively little is known about tandem repeat proteins formed by β hairpins. In this study, we discovered that the MORN repeats from MORN4 function as a protein binding module specifically recognizing a tail cargo binding region from Myo3a. The structure of the MORN4/Myo3a complex shows that MORN4 forms an extended single-layered β-sheet structure and uses a U-shaped groove to bind to the Myo3a tail with high affinity and specificity. Sequence and structural analyses further elucidated the unique sequence features for folding and target binding of MORN repeats. Our work establishes that the β-hairpin-based MORN repeats are protein-protein interaction modules.

INTRODUCTION

Tandem repeats (TRs) are ubiquitous in proteomes and estimated to occur in at least 14% of all proteins (Marcotte et al., 1999). The periodic sequence in these TRs can range from a few amino acids to large domains consisting of more than 100 residues. In the past several decades, TRs with lengths of 5–50 residues have attracted much attention since they can fold into particular three-dimensional structures capable of recognizing various targets including small molecules, nucleotides, short peptides, or large proteins (Kajava, 2012). TRs that form α-helical solenoids such as ankyrin repeats (ANK), tetratricopeptide repeats (TPR), armadillo repeats (ARM), and HEAT repeats are extensively studied (D'Andrea and Regan, 2003; Fung and Chook, 2014; Groves and Barford, 1999; Mosavi et al., 2004; Wang et al., 2014). In these proteins, each repeat is composed of two to three α helices and these repeats together fold into elongated, non-globular superhelices. α-Helix-based TRs have also been engineered for designated functions (Javadi and Itzhaki, 2013). For example, the designed ankyrin repeat proteins (DARPins) can be used as crystallization chaperones or high-affinity antibody mimetics (Binz et al., 2004; Pluckthun, 2015).

TRs with each repeat consisting of β hairpins are able to fold into various structures including β propellers (WD40 repeats, Kelch repeats), β helices (pentapeptide repeats, antifreeze proteins), β barrels, and single-layered β sheets (Roche et al., 2018). Though less studied, TRs that form single-layered β sheets are of special interest, since these proteins do not contain a well-formed interior hydrophobic core (Main et al., 2003). Only a few single-layered β-sheet TRs have been structurally characterized. One of them is the C terminus of centrosomal P4.1-associated protein (CPAP), also known as centromere protein J (CENP-J). The twisted elongated β sheet formed by the CPAP C-terminal 17 antiparallel β strands can bind to a proline-rich motif of another centrosomal protein called SCL-interrupting locus protein homolog (STIL) (Cottee et al., 2013; Hatzopoulos et al., 2013). Other examples include the outer surface protein A from *Borrelia burgdorferi*, bacterial biofilm forming proteins such as surface protein G from *Staphylococcus aureus*, and accumulation-associated protein from *Staphylococcus epidermidis* (Conrady et al., 2013; Gruszka et al., 2012; Makabe et al., 2008).

MORN repeats are another example of single-layered β sheet formed by β-hairpin TRs. It was first identified in junctophilins, a protein family that functions as a tether between plasma membranes and sarcoplasmic/ER membranes in excitable cells

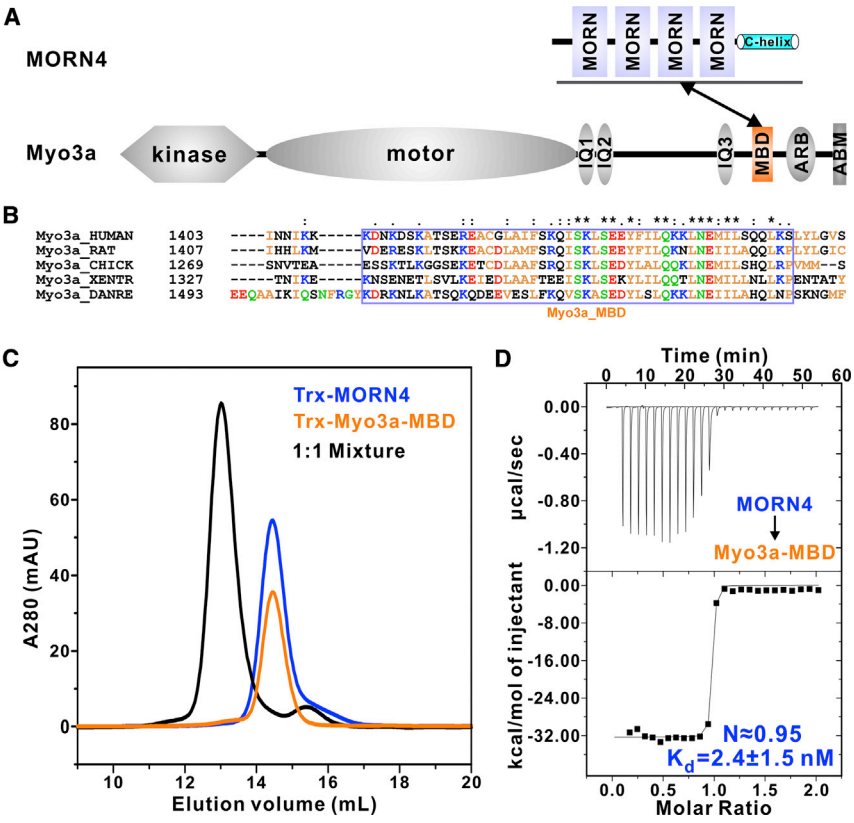

Figure 1. MORN4 Specifically Binds to Myo3a-MBD

(A) Domain organizations of MORN4 and Myo3a.

(B) Sequence alignment of Myo3a-MBD showing the high conservation of the domain among different species.

(C) Analytical gel-filtration results showing that MORN4 and Myo3a-MBD each adopt as a stable monomer. Mixing of the two proteins at a 1:1 ratio results in a homogeneous complex.

(D) ITC result showing that MORN4 binds to Myo3a-MBD with a very strong affinity and a 1:1 stoichiometry.

(Takeshima et al., 2000). The MORN repeats were named after their proposed function as "Membrane Occupation and Recognition Nexus." MORN repeats were later found in a number of other proteins including MORN1-5, SETD7, and plant PIPK, among others (Abnave et al., 2014; Bhattacharya et al., 2012; Cela et al., 2016; Ferguson et al., 2008; Ma et al., 2006; Wang et al., 2001). The only structural information of MORN repeats is from the structure of SETD7 (Wilson et al., 2002), a Lys methyltransferase for both histone and non-histone proteins (Pradhan et al., 2009). The six β-hairpin repeats situated at the N-terminal end of SETD7 form an elongated β sheet with a U-shaped groove, but the function of its MORN repeats remains unknown.

MORN4 and its *Drosophila* ortholog retinophilin (RTP) have been reported to be a binding partner/cargo of class III myosins (Lelli et al., 2016; Mecklenburg et al., 2015). MORN4 is highly conserved during evolution (Mecklenburg, 2007). Amino acid sequence analysis predicts that MORN4 contains four MORN repeats followed by a C-terminal α helix. MORN4 can co-localize with Myo3a at the tips of actin-based protrusions such as filopodia and stereocilia (Lelli et al., 2016). Similarly, RTP can bind to NINAC, the *Drosophila* ortholog of Myo3a, and localize to rhabdomere of *Drosophila* compound eyes (Mecklenburg et al., 2010; Venkatachalam et al., 2010). However, the molecular basis for MORN4/Myo3a interaction remains elusive.

In this work, we showed that MORN4 directly binds to the Myo3a tail with a dissociation constant (K_D) of ~2.4 nM. The crystal structure of MORN4/Myo3a complex revealed that MORN4 can use its highly conserved U-shaped groove to interact with Myo3a tail with high specificity. Disruption of the Myo3a and MORN4 interaction impairs filopodial tip localization of Myo3a in cells. Together with structure-based sequence analysis of MORN repeats from other proteins, we propose that MORN repeats are versatile protein-protein interaction modules.

RESULTS

MORN4 Binds to Myo3a Tail with a Very High Affinity

An earlier study showed that a highly conserved region specific in the tail of Myo3a, but not Myo3b, is responsible for MORN4 binding (Mecklenburg et al., 2015). This region (amino acids 1,410–1,457, denoted as MBD for MORN4 binding domain) is located between the putative IQ3 and the previously reported Espin1 binding site of the Myo3a tail (Figures 1A and 1B) (Dose et al., 2003; Liu et al., 2016). We used purified recombinant proteins to quantitatively characterize the binding. Both Trx-tagged full-length MORN4 and Myo3a-MBD were eluted as homogeneous monomers in an analytical gel-filtration column (Figure 1C). Mixing the two proteins at 1:1 ratio resulted in a homogeneous complex peak with a smaller elution volume (Figure 1C), suggesting that they formed a stable complex. An isothermal titration calorimetry (ITC)-based assay showed that the full-length MORN4 binds to Myo3a-MBD with an extremely high affinity (K_D ~ 2.4 nM) and a 1:1 stoichiometry (Figure 1D).

MORN4 Uses Its Conserved U-Shaped Groove to Interact with Myo3a-MBD

We solved the crystal structure of the MORN4/Myo3a-MBD complex at 1.55-Å resolution using the single-wavelength anomalous dispersion method by preparing iodine derivatives of the complex crystals (Table 1).

At this high resolution, nearly all residues of both molecules (L3-T146 for MORN4 and S1415-K1456 for Myo3a-MBD) were well resolved in the electron density map. Each MORN repeat (β2-β3, β4-β5, β6-β7, β8-β9) forms a curved β hairpin (Figure 2A). Residues preceding the first MORN repeat contain an additional β strand and structurally resemble half of the MORN repeat (i.e., the second strand of the β hairpin denoted as "MORN_N"). The C-terminal of the fourth MORN repeat also contains two

Table 1. Statistics of X-Ray Crystallographic Data Collection and Model Refinement

Datasets	Native	Iodine Derivative
Data Collection		
Wavelength (Å)	0.9791	1.5000
Space group	$P4_3$	$P4_3$
Unit cell parameters (Å)	$a = b = 73.7$, $c = 48.3$ $\alpha = \beta = \gamma = 90^\circ$	$a = b = 74.0$, $c = 47.9$ $\alpha = \beta = \gamma = 90^\circ$
Resolution range (Å)	50–1.55 (1.58–1.55)	50–1.70 (1.73–1.70)
No. of unique reflections	37,810 (1,914)	28,604 (1,434)
Redundancy	7.3 (7.2)	13.7 (13.9)
I/σ	37.2 (2.1)	71.4 (8.4)
Completeness (%)	99.9 (100)	100 (100)
R_{merge}[a] (%)	7.0 (113.8)	7.0 (42.4)
$CC_{1/2}$[b] (highest-resolution shell)	0.658	0.963
Structure Refinement		
Resolution (Å)	50–1.55 (1.61–1.55)	
R_{cryst}[c]/R_{free}[d] (%)	16.13/18.66 (20.67/24.01)	
RMSD bonds (Å)/angles (°)	0.007/0.931	
Average *B* factor[e]	25.6	
No. of atoms		
Protein atoms	1,552	
Ligands	44	
Water	133	
No. of reflections		
Working set	35,824 (3,582)	
Test set	1,961 (207)	
Ramachandran plot regions[e]		
Favored (%)	97.9	
Allowed (%)	2.1	
Outliers (%)	0	

Numbers in parentheses represent the value for the highest-resolution shell.

[a] $R_{merge} = \Sigma|I_i - \langle I \rangle|/\Sigma I_i$, where I_i is the intensity of measured reflection and $\langle I \rangle$ is the mean intensity of all symmetry-related reflections.

[b] $CC_{1/2}$ was defined by Karplus and Diederichs (2012).

[c] $R_{cryst} = \Sigma||F_{calc}| - |F_{obs}||/\Sigma F_{obs}$, where F_{obs} and F_{calc} are observed and calculated structure factors.

[d] $R_{free} = \Sigma_T||F_{calc}| - |F_{obs}||/\Sigma F_{obs}$, where T is a test dataset of about 5% of the total unique reflections randomly chosen and set aside prior to refinement.

[e] *B* factors and Ramachandran plot statistics are calculated using MolProbity (Chen et al., 2010).

additional β strands. They form a β hairpin, and are referred to as "MORN-C." MORN_N and MORN-C can be viewed as capping elements to stabilize the MORN repeats 1 and 4, respectively (Figures 2A–2C). All 11 curved β strands together with the fingers in each β hairpin form a single-layered β sheet with a U-shaped groove, similar to the overall architecture of the SETD7 MORN repeats (Wilson et al., 2002). This U-shaped groove snugly accommodates an elongated α helix formed by Myo3a-MBD, burying a total surface area of ~1,500 Å^2 (calculated using the PISA server [Krissinel and Henrick, 2007]). Sequence conservation analysis of vertebrate MORN4 and *Drosophila* RTP revealed that residues located at the surface of Myo3a-MBD binding groove are highly conserved (Figures 2D and S1), suggesting that *Drosophila* RTP also uses this groove to bind to NINAC. The very C terminus of MORN4 forms an α helix (C helix) and packs to the back side of the U-shaped groove. Charge-charge interactions (E63-R142), hydrogen bonds (E63-S138 and E86-Q135), and hydrophobic interactions (L99-V131) mediate the interaction between the C helix and the β sheet (Figure 2E). The interaction of the C helix with the MORN repeat β sheet generates some sort of folding core for the full-length MORN4 and therefore may stabilize the overall folding of the protein. Indeed, substitution of E63 with Leu, which would affect the coupling between the C helix and the β sheet (Figure 2E), destabilized the folding of MORN4 in a heat-induced (Figures 2F and S2) and urea-induced (data not shown) denaturation assays. The E63-to-Leu mutation also impaired the interaction between MORN4 and Myo3a-MBD (Figure 2G).

Detailed Interaction between MORN4 and Myo3a-MBD

The surface of the U-shaped groove of MORN4 is mainly hydrophobic formed by a number of aromatic or bulky hydrophobic residues including F8, Y10, F33, F48, F56, F77, and M83. Correspondingly, an array of hydrophobic residues along one side of the Myo3a-MBD α helix (F1428, I1432, L1435, Y1439, L1442, and L1446) combined with the C-terminal loop (I1450 and L1455) face toward this surface, forming extensive hydrophobic contacts (Figure 3A). In addition, the β-hairpin fingers of MORN4 are also extensively involved in binding by forming several pairs of hydrogen bonds with Myo3a-MBD, presumably further enhancing binding affinity and specificity (Figure 3A). Notably, three Gly residues (G23, G69, and G92) located at the tip of the first, third, and fourth MORN repeat β-hairpin fingers use their backbone carbonyl to form hydrogen bonds with backbone amide (I1450) or side chains (S1436, Q1443) of Myo3a-MBD. The side chain of N119 at the tip of the MORN-C β-hairpin finger forms hydrogen bonds with S1429. G46 at the tip of the second MORN repeat β-hairpin finger forms another hydrogen bond with the side chain of R25 from MORN4 itself. These five hydrogen bonds likely play critical roles in wrapping the Myo3a-MBD α helix in the U-shaped groove of the MORN repeats (Figure 3A).

We performed a series of mutagenesis experiments to validate the interactions observed in the MORN4/Myo3a-MBD crystal structure (Figure 3B). ITC-based binding assays showed that substituting the hydrophobic residues (F33, F56, or F77) at the MORN4 groove with polar residue Gln individually led to a few-fold to tens-of-fold decrease in binding affinity. We also tested roles of the hydrogen bonds in the interaction. Mutations of polar residues from Myo3a-MBD (Q1443 or N1447) to Ala or R25 from MORN4 to aromatic Phe also significantly weakened the binding.

With this high-resolution structure in hand, we hoped to design a mutation that can dramatically affect or even abolish the binding for further functional studies of the MORN4 and Myo3a interaction in cells. We noticed that F1428 from Myo3a-MBD, which inserts deep into the MORN4 groove, is close to a positively charged residue R79 (Figure 3A). We anticipated that by

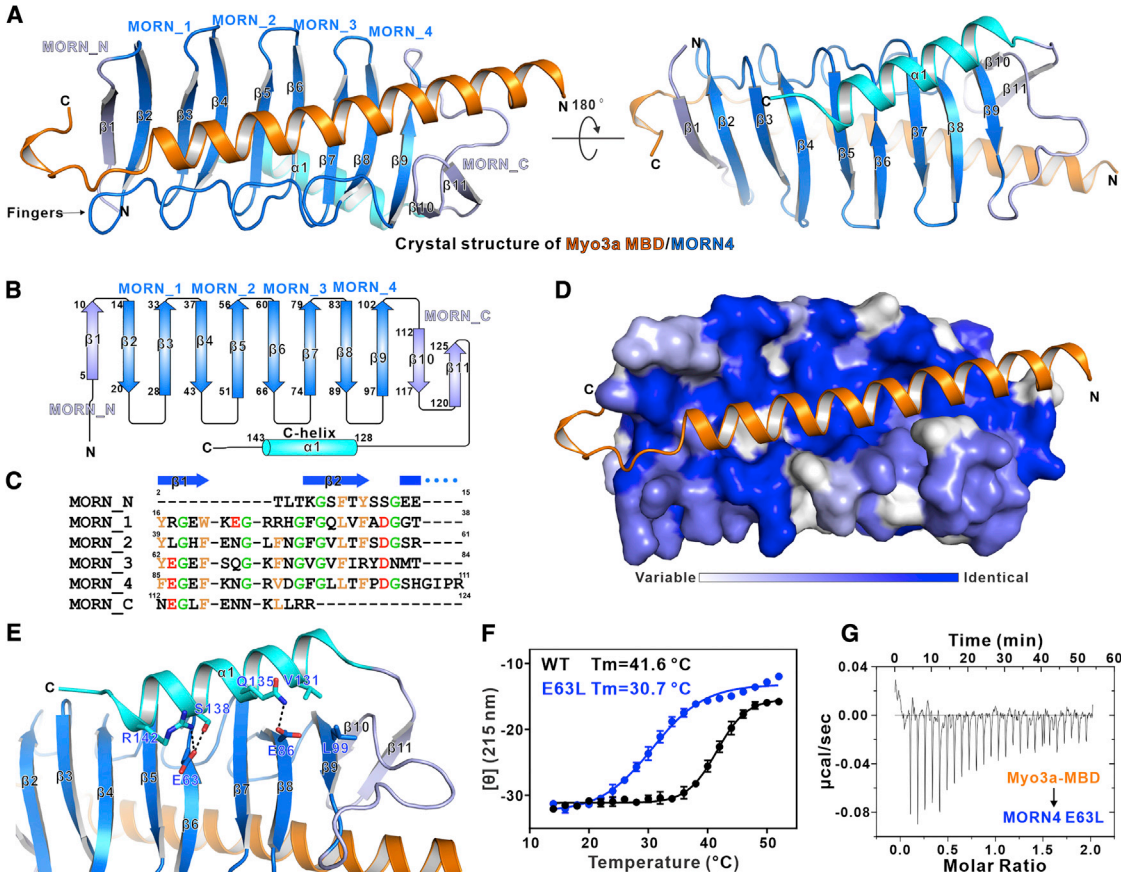

Figure 2. MORN4 Uses Its U-Shaped Groove to Bind to Myo3a-MBD

(A) Ribbon representations of the MORN4/Myo3a-MBD complex crystal structure. The MORN repeats of MORN4 are colored light and dark blue, and the C helix is colored cyan. Myo3a-MBD is colored orange. This coloring scheme is used throughout the paper.

(B) Secondary structure topology showing the MORN repeats β-sheet arrangement.

(C) Sequence alignment of the MORN repeats of MORN4 together with the two capping repeats MORN_N and MORN_C.

(D) The amino acid conservation map of MORN4. The conservation map was calculated based on the sequence alignment of vertebrates MORN4 and *Drosophila* RTP as shown in Figure S1. The identical residues are colored dark blue, the strongly similar residues are colored blue, the weakly similar residues are colored light blue, and the variable residues are colored white.

(E) Detailed interactions between the C helix and the MORN repeats. The side chains of the residues involved in the interactions are highlighted in the stick model. Charge-charge and hydrogen-bonding interactions are highlighted by dashed lines.

(F) Thermal denaturation profiles of MORN4 WT and E63L by plotting the ellipticity values of the protein at 215 nm as a function of temperature (see Figure S2 for the representative CD spectra at different temperatures). The melting temperatures were calculated by fitting the curves using the sigmoid function.

(G) ITC result showing that the MORN4 E63L mutant had very weak binding to Myo3a-MBD.

mutating F1428 to Arg, the repulsion force by the introduced positively charged residue might greatly impair the binding. Consistent with our prediction, Myo3a-MBD F1428R can largely weaken the interaction between Myo3a-MBD and MORN4 with a K_D of about 51 μM, a more than 20,000-fold reduction in the binding affinity (Figure 3B).

MORN4 was reported to locate at the tip of filopodia dependent on Myo3a binding (Mecklenburg et al., 2015). Myo3a has previously been shown to regulate actin protrusion dynamics (Raval et al., 2016). We used the filopodia tip localization assay to test our structural finding and determine the impact of MORN4 binding on Myo3a's ability to regulate actin protrusion length. Myo3a alone can localize at the tip of filopodia in COS7 cells (Figures 3C and 3D; see also Les Erickson et al., 2003; Liu et al., 2016; Raval et al., 2016; Salles et al., 2009). When WT MORN4 was co-transfected with Myo3a, MORN4 co-localized with Myo3a at the tip of filopodia and further promoted the filopodia tip enrichment of Myo3a (Figures 3C and 3D; see also Mecklenburg et al., 2015). In contrast, when MORN4 was co-transfected with Myo3a-F1428R, the filopodia tip localization of MORN4 was largely diminished (Figures 3C and 3D). The mutant Myo3a was still enriched at the tips of filopodia, although the expression of MORN4 did not further promote the filopodia tip enrichment of Myo3a-F1428R (Figures 3C and 3D).

Structural Signature of MORN Repeats

The MORN4/Myo3a-MBD complex structure is the first atomic model showing how MORN-repeat-containing proteins recognize their targets (Figure 4A). It provides us an opportunity to analyze the structural determinants of MORN repeats for folding

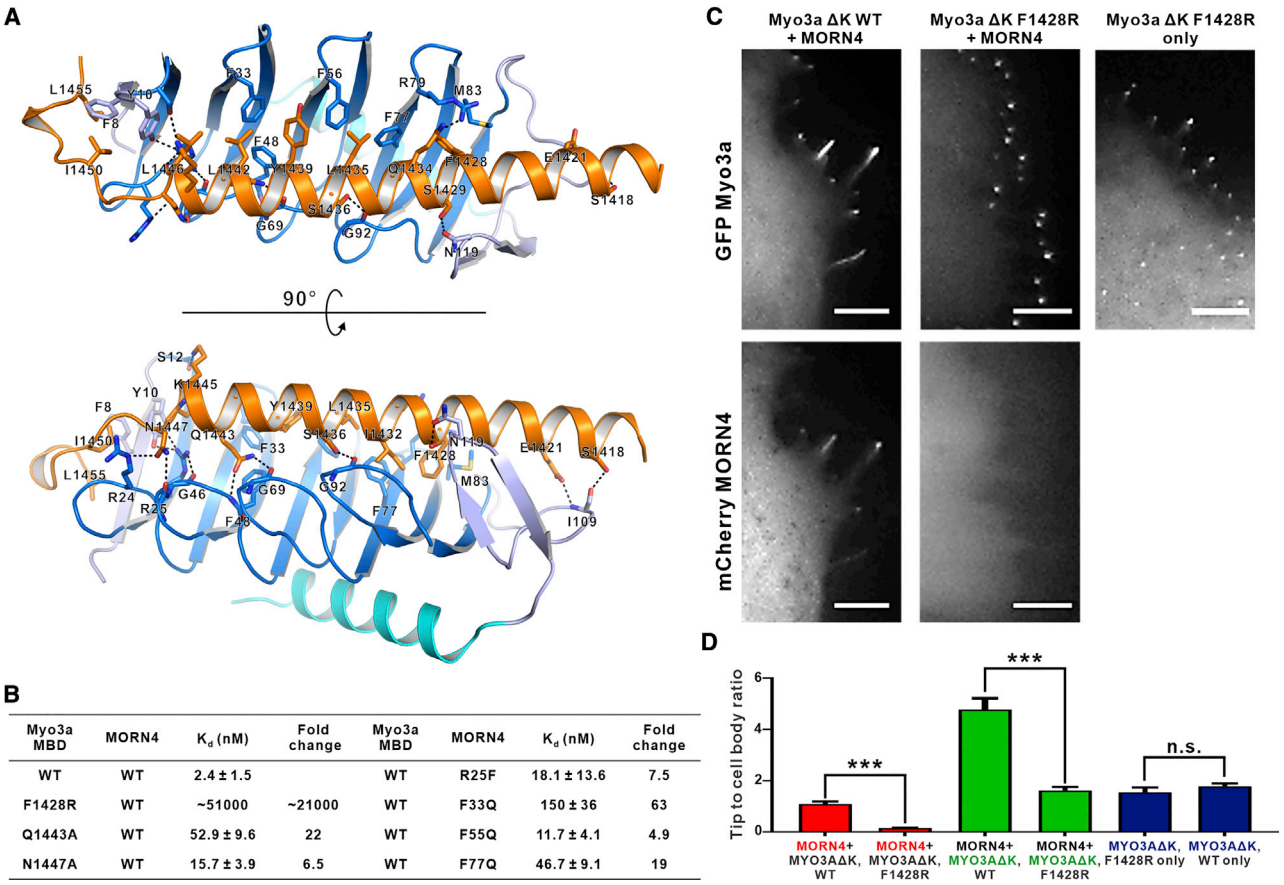

B

Myo3a MBD	MORN4	K_d (nM)	Fold change	Myo3a MBD	MORN4	K_d (nM)	Fold change
WT	WT	2.4 ± 1.5		WT	R25F	18.1 ± 13.6	7.5
F1428R	WT	~51000	~21000	WT	F33Q	150 ± 36	63
Q1443A	WT	52.9 ± 9.6	22	WT	F55Q	11.7 ± 4.1	4.9
N1447A	WT	15.7 ± 3.9	6.5	WT	F77Q	46.7 ± 9.1	19

Figure 3. Detailed Interactions between MORN4 and Myo3a-MBD

(A) Detailed interaction between MORN4 and Myo3a-MBD. The side chains or main chains of the residues involved in the interactions are highlighted in the stick model. Charge-charge and hydrogen-bonding interactions are highlighted by dashed lines.

(B) Summary of ITC-derived dissociation constants showing the impact of mutating the interface residues on the formation of the complex.

(C) Representative fluorescence images of COS7 cells co-expressing mCherry-MORN4 and WT or mutant GFP-Myo3a. Scale bars, 5 μm.

(D) Quantifications of the tip to cell body ratios of GFP-Myo3aΔK (or its mutants) and mCherry-MORN4 when expressed in COS7 cells. mCherry-MORN4 co-expression with GFP-Myo3aΔK led to a greater tip localization of mCherry-MORN4 compared with its co-expression with GFP-Myo3aΔK, F1428R ($p < 0.001$; t test). Similarly, GFP-Myo3aΔK demonstrated significantly higher tip localization compared with GFP-Myo3aΔK, F1428R when co-expressed with mCherry-MORN4 ($p < 0.001$; t test). There was no difference in the tip localization ability of GFP-Myo3aΔK and GFP-Myo3aΔK, F1428R when expressed in the absence of mCherry-MORN4. Data are represented as mean ± SEM. For each group, at least 30 cells (i.e., $n > 30$) from three or more different batches of experiments were quantified. ***$p < 0.001$; n.s., not significant ($p > 0.05$).

and target binding. Each MORN repeat generally contains 23–26 amino acids that form a β-hairpin structure. MORN4 contains four typical MORN repeats, each with a consensus sequence motif and two incomplete or atypical MORN repeats (MORN_N and MORN_C) capping at the N terminus and C terminus, respectively (Figure 4C). Six MORN repeats can be identified in SETD7, and again the sequences of the first and last repeats deviate from the consensus sequence somewhat, likely due to the capping role of the two repeats (Figures 4B and 4C).

Although extended β-sheet structures lack a well-defined hydrophobic folding core, hydrophobic interactions are likely indispensable for the folding of MORN repeats. In each MORN repeat, aromatic residues at the position 1 of the first β strand (Y16, Y39, Y62, and F85 in β2, β4, β6, and β8, respectively) form hydrophobic interaction or cation-π stacking with the residue at the position 10 in the hairpin finger (R25, F48, F71, and V94, respectively); aromatic residue at position 5 of the first β strand (W20, F43, Y66, and F89 at the ends of β2, β4, β6, and β8, respectively) form an elongated and continuous hydrophobic surface for binding to Myo3a-MBD (Figures 4A and 4C). The residues in the 1, 5, and 10 positions in the SETD7 MORN repeats also follow the pattern as seen in MORN4, so the hydrophobic interactions among these residues are likely to be important for the folding of SETD7 MORN repeats (Figures 4B and 4C).

Gly residues are highly preferred at some positions in MORN repeats (Figure 4C). Gly at position 8 (the third residue in each β-hairpin finger) is structurally required for the tip of the finger to interact with the target protein (Figure 3A). Two Gly residues preceding the first and the second β strand (at positions 12 and 21) are required to make the sharp turns, as only Gly can adopt the unusual dihedral angles at these two positions. It is unique that both β strands in each MORN repeat contain a

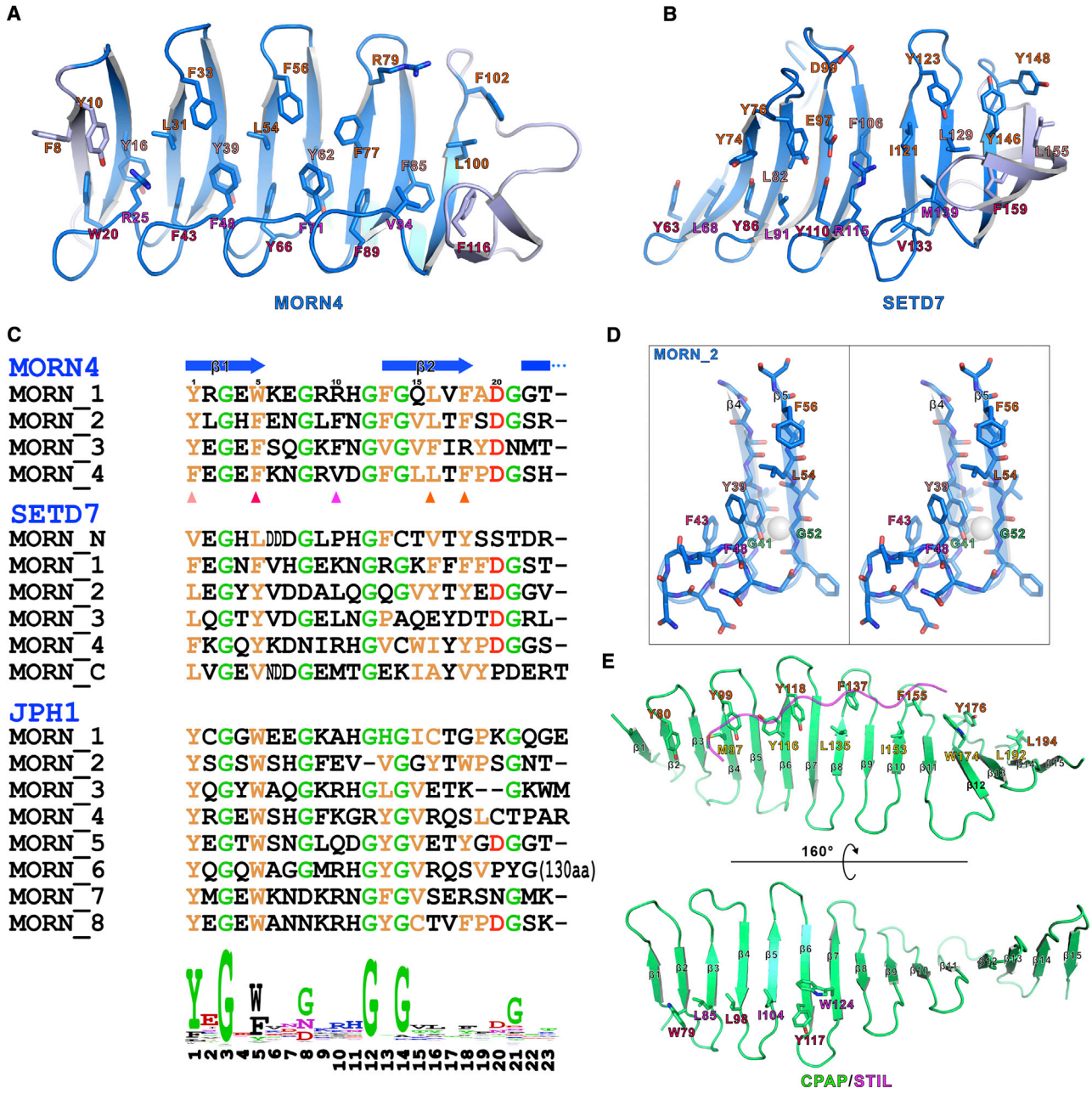

Figure 4. Structural Features of MORN Repeats

(A and B) Combined stick and ribbon representations of MORN4 (A) and SETD7 MORN repeats (B, PDB: 1H3I) structures showing the residues critical for the folding of MORN repeats and for potential target binding.

(C) Sequence alignment of MORN repeats from MORN4, SETD7, and junctophilin1. The sequence logo was generated based on the alignments of all MORN repeats found in human proteins.

(D) Stereo view of combined stick and ribbon representations of the second MORN repeat of MORN4 showing the space freed up by the Gly residue in the middle of each β strand for bulky residues in the positions 1, 5, and 10 to interact with each other. The putative Cβs are shown as transparent gray spheres to indicate that there is no room to accommodate any other residues besides Gly in these two positions.

(E) Combined stick and ribbon representations of CPAP/STIL complex structure (PDB: 4BY2) showing the residues critical for CPAP β-sheet folding or target binding.

conserved Gly in the middle (the Gly residues in the positions 3 and 14; Figure 4C). The lack of side chain of these two Gly residues provides necessary space for the hydrophobic side chains from residues in the 1, 5, and 10 positions in each MORN repeat to interact with each other (Figure 4D).

Hydrophobic residues are also favored at positions 16 and 18 in each MORN repeat, and these two residues are situated at the end of the second β strand and facing the target binding groove (Figure 4C). In the MORN4/Myo3a-MBD complex, these hydrophobic residues play critical roles in binding to hydrophobic

amino acids from Myo3a-MBD (Figure 3A). Our mutagenesis experiments showed that substitutions of each of these residues (e.g., F33, F56, and F77) with a polar Gln invariably weakened its binding to Myo3a-MBD (Figure 3B). SETD7 MORN repeats also contain such an array of hydrophobic residues, with the exception that negatively charged residues are in these two positions in the third MORN repeat (Figures 4B and 4C). Based on this analysis, we propose that SETD7 MORN repeats may also use its U-shaped groove to bind to target protein(s).

Some of the features seen in the MORN repeat structures are also found in other single-layered β-sheet structures. The structure of CPAP/STIL complex is an example (Figure 4E). Instead of forming a U-shaped groove for target binding seen in MORN4, CPAP forms a twisted β sheet and uses the flat surface on one side to recognize its binding partner STIL. Similar to the hydrophobic interface in the MORN4/Myo3a-MBD complex structure, a row of hydrophobic residues are aligned together at one end of the second β strand of each β hairpin in the CPAP/STIL complex. The STIL peptide only covers two-thirds of the entire row of hydrophobic residues, implying that there might be other target(s) utilizing this unoccupied surface. Interstrand hydrophobic interactions are likely important for the folding of CPAP as well. On the opposite side of the binding interface, another row of hydrophobic residues are presumably critical for stabilizing the β-sheet fold of CPAP.

DISCUSSION

In contrast to the relatively abundant knowledge on α-helix TRs, β-strand TRs have received much less attention. In the current study, we characterized structural and target binding properties of a β-strands-only TR protein, MORN4. MORN repeats are found in more than a dozen proteins that play important roles in many biological processes such as tethering ER to plasma membranes, catalyzing methylation of proteins, and modulating filopodial development of cells (Mecklenburg et al., 2015; Takeshima et al., 2000; Wang et al., 2001). The structure of MORN4/Myo3a complex presented in this study, together with the previously reported SETD7 structure (Wilson et al., 2002), revealed that MORN repeats fold into a single-layered β-sheet structure with a U-shaped target binding groove.

When initially discovered in junctophilins, MORN repeats were suggested to bind to lipid membranes (Takeshima et al., 2000). The structures of MORN4 and SETD7, however, do not support a membrane binding role for the MORN repeats of these two proteins, as neither of these two MORN repeats contains obvious positively charged surfaces (Figures S3A and S3B). Consistent with this structure analysis, we could not detect any lipid membrane binding for MORN4 using a liposome sedimentation assay (Figure S3C). Instead, our structure-based sequence analysis of MORN repeats showed that most of the residues defining the MORN repeats are located in the U-shaped groove to form a hydrophobic surface. These residues are likely to be important for MORN repeat folding and target binding (Figure 4). It is noted that the β-hairpin fingers of MORN repeats, which are more variable among different MORN-repeat-containing proteins (Figure 4C), are directly involved in binding to target proteins (Figure 3A). Therefore, it is anticipated that the residues in the β-hairpin fingers can actively contribute to the target binding specificity. Consistent with this analysis, the residues in the β-hairpin fingers of SETD7 MORN repeats are enriched in negatively charged amino acids (Figure 4C), and SETD7 MORN repeats can bind to a panel of positively charged DNA binding proteins (our unpublished data).

Although β strands can be utilized as the basic folding unit, structures of single-layered β-sheet proteins are quite different from β-barrel and β-propeller proteins. For β barrels and β propellers with enclosed β-sheet packings, each of these proteins contains a hydrophobic folding core. Instead, in the single-layered β-sheet protein, interstrand hydrophobic interactions between neighboring strands are likely to be important for the folding, although such interactions sometimes are not sufficient for stable folding in these proteins. In the MORN4 structure, the interaction of the C helix with the β-sheet surface opposite to the U-shaped groove contributes to the stability of the protein (Figure 2). In the SETD7 MORN structure, a very long curved β-strand C-terminal to the last MORN repeat (Figure 4B, colored light blue) is coupled to the back side of the U-shaped groove. This long curved β strand may stabilize the MORN repeats structure. CPAP probably uses a slightly different strategy. A number of interstrand hydrophobic interactions on the back side of the target binding surface may play a role in stabilizing the extended β sheet of CPAP (residues shown in the explicit model in the lower panel of Figure 4E). More structural work on other single-layered β-sheet proteins will be helpful in further consolidating the general features of the folding and target recognition mechanisms of this category of TR proteins.

STAR★METHODS

Detailed methods are provided in the online version of this paper and include the following:

- KEY RESOURCES TABLE
- CONTACT FOR REAGENT AND RESOURCE SHARING
- EXPERIMENTAL MODEL AND SUBJECT DETAILS
  - COS7 Cells Culture
- METHOD DETAILS
  - Constructs and Protein Purification
  - Analytical Gel Filtration Chromatography
  - Isothermal Titration Calorimetry Assay
  - Crystallography
  - Circular Dichroism Spectroscopy Based Thermal Denaturation
  - Liposome-Binding Assay
  - COS7 Cell Culture, Transfection and Imaging
- QUANTIFICATION AND STATISTICAL ANALYSIS
- DATA AND CODE AVAILABILITY
  - Data Resources

SUPPLEMENTAL INFORMATION

Supplemental Information can be found online at https://doi.org/10.1016/j.str.2019.06.004.

ACKNOWLEDGMENTS

We thank the Shanghai Synchrotron Radiation Facility beamlines BL17U1 and BL19U1 for X-ray beam time. This work was supported by a grant

from RGC of Hong Kong (16149516) to M.Z., grants from the National Natural Science Foundation of China (nos. 31670765 and 31870746 to W.L. and 31700673 to H.L.) and grants from Shenzhen Basic Research Grants (JCYJ20160229153100269 to M.Z. and JCYJ20170411090807530 to W.L.). M.Z. is a Kerry Holdings Professor in Science and a Senior Fellow of IAS at HKUST.

AUTHOR CONTRIBUTIONS

J.L., H.L., and M.H.R. performed experiments. J.L., H.L., M.H.R., J.W., C.M.Y., W.L., and M.Z. analyzed data. J.L., H.L., W.L., and M.Z. designed the research. J.L., H.L., and M.Z. drafted the paper, and all authors commented on the paper. M.Z. coordinated the project.

DECLARATION OF INTERESTS

The authors declare no competing interests.

Received: April 5, 2019
Revised: May 25, 2019
Accepted: June 17, 2019
Published: July 03, 2019

REFERENCES

Abnave, P., Mottola, G., Gimenez, G., Boucherit, N., Trouplin, V., Torre, C., Conti, F., Ben Amara, A., Lepolard, C., Djian, B., et al. (2014). Screening in planarians identifies MORN2 as a key component in LC3-associated phagocytosis and resistance to bacterial infection. Cell Host Microbe *16*, 338–350.

Adams, P.D., Afonine, P.V., Bunkoczi, G., Chen, V.B., Davis, I.W., Echols, N., Headd, J.J., Hung, L.W., Kapral, G.J., Grosse-Kunstleve, R.W., et al. (2010). PHENIX: a comprehensive Python-based system for macromolecular structure solution. Acta Crystallogr. D Biol. Crystallogr. *66*, 213–221.

Bhattacharya, M.R., Gerdts, J., Naylor, S.A., Royse, E.X., Ebstein, S.Y., Sasaki, Y., Milbrandt, J., and DiAntonio, A. (2012). A model of toxic neuropathy in *Drosophila* reveals a role for MORN4 in promoting axonal degeneration. J. Neurosci. *32*, 5054–5061.

Binz, H.K., Amstutz, P., Kohl, A., Stumpp, M.T., Briand, C., Forrer, P., Grutter, M.G., and Pluckthun, A. (2004). High-affinity binders selected from designed ankyrin repeat protein libraries. Nat. Biotechnol. *22*, 575–582.

Cela, P., Hampl, M., Fu, K.K., Kunova Bosakova, M., Krejci, P., Richman, J.M., and Buchtova, M. (2016). MORN5 expression during craniofacial development and its interaction with the BMP and TGFbeta pathways. Front. Physiol. *7*, 378.

Chen, V.B., Arendall, W.B., 3rd, Headd, J.J., Keedy, D.A., Immormino, R.M., Kapral, G.J., Murray, L.W., Richardson, J.S., and Richardson, D.C. (2010). MolProbity: all-atom structure validation for macromolecular crystallography. Acta Crystallogr. D Biol. Crystallogr. *66*, 12–21.

Conrady, D.G., Wilson, J.J., and Herr, A.B. (2013). Structural basis for Zn^{2+}-dependent intercellular adhesion in staphylococcal biofilms. Proc. Natl. Acad. Sci. U S A *110*, E202–E211.

Cottee, M.A., Muschalik, N., Wong, Y.L., Johnson, C.M., Johnson, S., Andreeva, A., Oegema, K., Lea, S.M., Raff, J.W., and van Breugel, M. (2013). Crystal structures of the CPAP/STIL complex reveal its role in centriole assembly and human microcephaly. Elife *2*, e01071.

D'Andrea, L.D., and Regan, L. (2003). TPR proteins: the versatile helix. Trends Biochem. Sci. *28*, 655–662.

Dose, A.C., Hillman, D.W., Wong, C., Sohlberg, L., Lin-Jones, J., and Burnside, B. (2003). Myo3A, one of two class III myosin genes expressed in vertebrate retina, is localized to the calycal processes of rod and cone photoreceptors and is expressed in the sacculus. Mol. Biol. Cell *14*, 1058–1073.

Emsley, P., Lohkamp, B., Scott, W.G., and Cowtan, K. (2010). Features and development of Coot. Acta Crystallogr. D Biol. Crystallogr. *66*, 486–501.

Ferguson, D.J., Sahoo, N., Pinches, R.A., Bumstead, J.M., Tomley, F.M., and Gubbels, M.J. (2008). MORN1 has a conserved role in asexual and sexual development across the apicomplexa. Eukaryot. Cell *7*, 698–711.

Fung, H.Y., and Chook, Y.M. (2014). Atomic basis of CRM1-cargo recognition, release and inhibition. Semin. Cancer Biol. *27*, 52–61.

Groves, M.R., and Barford, D. (1999). Topological characteristics of helical repeat proteins. Curr. Opin. Struct. Biol. *9*, 383–389.

Gruszka, D.T., Wojdyla, J.A., Bingham, R.J., Turkenburg, J.P., Manfield, I.W., Steward, A., Leech, A.P., Geoghegan, J.A., Foster, T.J., Clarke, J., et al. (2012). Staphylococcal biofilm-forming protein has a contiguous rod-like structure. Proc. Natl. Acad. Sci. U S A *109*, E1011–E1018.

Hatzopoulos, G.N., Erat, M.C., Cutts, E., Rogala, K.B., Slater, L.M., Stansfeld, P.J., and Vakonakis, I. (2013). Structural analysis of the G-box domain of the microcephaly protein CPAP suggests a role in centriole architecture. Structure *21*, 2069–2077.

Javadi, Y., and Itzhaki, L.S. (2013). Tandem-repeat proteins: regularity plus modularity equals design-ability. Curr. Opin. Struct. Biol. *23*, 622–631.

Kajava, A.V. (2012). Tandem repeats in proteins: from sequence to structure. J. Struct. Biol. *179*, 279–288.

Karplus, P.A., and Diederichs, K. (2012). Linking crystallographic model and data quality. Science *336*, 1030–1033.

Krissinel, E., and Henrick, K. (2007). Inference of macromolecular assemblies from crystalline state. J. Mol. Biol. *372*, 774–797.

Lelli, A., Michel, V., Boutet de Monvel, J., Cortese, M., Bosch-Grau, M., Aghaie, A., Perfettini, I., Dupont, T., Avan, P., El-Amraoui, A., et al. (2016). Class III myosins shape the auditory hair bundles by limiting microvilli and stereocilia growth. J. Cell Biol. *212*, 231–244.

Les Erickson, F., Corsa, A.C., Dose, A.C., and Burnside, B. (2003). Localization of a class III myosin to filopodia tips in transfected HeLa cells requires an actin-binding site in its tail domain. Mol. Biol. Cell *14*, 4173–4180.

Liu, H., Li, J., Raval, M.H., Yao, N., Deng, X., Lu, Q., Nie, S., Feng, W., Wan, J., Yengo, C.M., et al. (2016). Myosin III-mediated cross-linking and stimulation of actin bundling activity of Espin. Elife *5*, https://doi.org/10.7554/eLife.12856.

Ma, H., Lou, Y., Lin, W.H., and Xue, H.W. (2006). MORN motifs in plant PIPKs are involved in the regulation of subcellular localization and phospholipid binding. Cell Res. *16*, 466–478.

Main, E.R., Jackson, S.E., and Regan, L. (2003). The folding and design of repeat proteins: reaching a consensus. Curr. Opin. Struct. Biol. *13*, 482–489.

Makabe, K., Biancalana, M., Yan, S., Tereshko, V., Gawlak, G., Miller-Auer, H., Meredith, S.C., and Koide, S. (2008). High-resolution structure of a self-assembly-competent form of a hydrophobic peptide captured in a soluble beta-sheet scaffold. J. Mol. Biol. *378*, 459–467.

Marcotte, E.M., Pellegrini, M., Yeates, T.O., and Eisenberg, D. (1999). A census of protein repeats. J. Mol. Biol. *293*, 151–160.

Mecklenburg, K.L. (2007). Drosophila retinophilin contains MORN repeats and is conserved in humans. Mol. Genet. Genomics *277*, 481–489.

Mecklenburg, K.L., Freed, S.A., Raval, M., Quintero, O.A., Yengo, C.M., and O'Tousa, J.E. (2015). Invertebrate and vertebrate class III myosins interact with MORN repeat-containing adaptor proteins. PLoS One *10*, e0122502.

Mecklenburg, K.L., Takemori, N., Komori, N., Chu, B., Hardie, R.C., Matsumoto, H., and O'Tousa, J.E. (2010). Retinophilin is a light-regulated phosphoprotein required to suppress photoreceptor dark noise in *Drosophila*. J. Neurosci. *30*, 1238–1249.

Mosavi, L.K., Cammett, T.J., Desrosiers, D.C., and Peng, Z.Y. (2004). The ankyrin repeat as molecular architecture for protein recognition. Protein Sci. *13*, 1435–1448.

Otwinowski, Z., and Minor, W. (1997). Processing of X-ray diffraction data collected in oscillation mode. Methods Enzymol. *276*, 307–326.

Pluckthun, A. (2015). Designed ankyrin repeat proteins (DARPins): binding proteins for research, diagnostics, and therapy. Annu. Rev. Pharmacol. Toxicol. *55*, 489–511.

Pradhan, S., Chin, H.G., Esteve, P.O., and Jacobsen, S.E. (2009). SET7/9 mediated methylation of non-histone proteins in mammalian cells. Epigenetics *4*, 383–387.

Raval, M.H., Quintero, O.A., Weck, M.L., Unrath, W.C., Gallagher, J.W., Cui, R., Kachar, B., Tyska, M.J., and Yengo, C.M. (2016). Impact of the motor

and tail domains of class III myosins on regulating the formation and elongation of actin protrusions. J. Biol. Chem. *291*, 22781–22792.

Roche, D.B., Viet, P.D., Bakulina, A., Hirsh, L., Tosatto, S.C.E., and Kajava, A.V. (2018). Classification of beta-hairpin repeat proteins. J. Struct. Biol. *201*, 130–138.

Salles, F.T., Merritt, R.C., Jr., Manor, U., Dougherty, G.W., Sousa, A.D., Moore, J.E., Yengo, C.M., Dose, A.C., and Kachar, B. (2009). Myosin IIIa boosts elongation of stereocilia by transporting espin 1 to the plus ends of actin filaments. Nat. Cell Biol. *11*, 443–450.

Takeshima, H., Komazaki, S., Nishi, M., Iino, M., and Kangawa, K. (2000). Junctophilins: a novel family of junctional membrane complex proteins. Mol. Cell *6*, 11–22.

Venkatachalam, K., Wasserman, D., Wang, X., Li, R., Mills, E., Elsaesser, R., Li, H.S., and Montell, C. (2010). Dependence on a retinophilin/myosin complex for stability of PKC and INAD and termination of phototransduction. J. Neurosci. *30*, 11337–11345.

Wang, C., Wei, Z.Y., Chen, K.Y., Ye, F., Yu, C., Bennett, V., and Zhang, M.J. (2014). Structural basis of diverse membrane target recognitions by ankyrins. Elife *3*, https://doi.org/10.7554/eLife.04353.

Wang, H., Cao, R., Xia, L., Erdjument-Bromage, H., Borchers, C., Tempst, P., and Zhang, Y. (2001). Purification and functional characterization of a histone H3-lysine 4-specific methyltransferase. Mol. Cell *8*, 1207–1217.

Wilson, J.R., Jing, C., Walker, P.A., Martin, S.R., Howell, S.A., Blackburn, G.M., Gamblin, S.J., and Xiao, B. (2002). Crystal structure and functional analysis of the histone methyltransferase SET7/9. Cell *111*, 105–115.

Ye, F., Huang, Y., Li, J., Ma, Y., Xie, C., Liu, Z., Deng, X., Wan, J., Xue, T., Liu, W., et al. (2018). An unexpected INAD PDZ tandem-mediated plcbeta binding in *Drosophila* photo receptors. Elife *7*, https://doi.org/10.7554/eLife.41848.

STAR★METHODS

KEY RESOURCES TABLE

REAGENT or RESOURCE	SOURCE	IDENTIFIER
Chemicals, Peptides, and Recombinant Proteins		
Dulbecco's Modified Eagle Medium (DMEM)	Thermo Fisher Scientific	Cat#11995065
fetal bovine serum (FBS)	Thermo Fisher Scientific	Cat#16000044
penicillin-streptomycin	Thermo Fisher Scientific	Cat#15140122
Brain lipid extracts	Sigma	Cat#B1502
Recombinant protein: Mouse MORN4 WT (full length, ref# NP_932776.1)	This paper	N/A
Recombinant protein: Human Myo3a MBD WT (aa: 1410-1457, ref# NP_059129.3)	This paper	N/A
Recombinant protein: Drosophila Norpa CC-PBM WT (aa: 863-1095, ref#NP_525069.2)	(Ye et al., 2018)	N/A
Critical Commercial Assays		
FUGENE HD transfection agent	Promega	Cat#E2131
Deposited Data		
Crystal structure of MORN4/Myo3a MBD	This paper	PDB: 6JLE
Crystal structure of SETD7	(Wilson et al., 2002)	PDB: 1H3I
Crystal structure of CPAP/STIL complex	(Cottee et al., 2013)	PDB: 4BY2
Experimental Models: Cell Lines		
Human: COS7 cells	ATCC	CRL-1651; RRID: CVCL_0224
Experimental Models: Organisms/Strains		
Escherichia coli: BL21 (DE3)	Invitrogen	Cat#C600003
Recombinant DNA		
Plasmid: mCherry-MORN4	(Mecklenburg et al., 2015)	N/A
Plasmid: GFP-Myo3aΔK	(Mecklenburg et al., 2015)	N/A
Plasmid: pET32M.3C Mouse MORN4	This paper	N/A
Plasmid: pET32M.3C Human Myo3a MBD	This paper	N/A
Software and Algorithms		
Origin7.0 & OriginPro 8.0	OriginLab	http://www.originlab.com/
HKL2000 & HKL3000	(Otwinowski and Minor, 1997)	http://www.hkl-xray.com/
Coot	(Emsley et al., 2010)	http://www2.mrc-lmb.cam.ac.uk/Personal/pemsley/coot/
PHENIX	(Adams et al., 2010)	http://www.phenix-online.org/
MolProbity	(Chen et al., 2010)	http://molprobity.biochem.duke.edu/
PyMOL	DeLano Scientific LLC	http://www.pymol.org/
ImageJ	NIH	https://imagej.nih.gov/ij/

CONTACT FOR REAGENT AND RESOURCE SHARING

Further information and requests for reagents may be directed to, and will be fulfilled by the Lead Contact Mingjie Zhang (mzhang@ust.hk).

EXPERIMENTAL MODEL AND SUBJECT DETAILS

COS7 Cells Culture

COS7 cells which are derived from the kidney of a male adult African green monkey (from ATCC) were cultured in DMEM (Invitrogen) supplemented with 4 mM L-glutamine, 1 mM Sodium Pyruvate, 4.5 g/L D-Glucose, 10% fetal bovine serum, and 100 units of

penicillin-streptomycin. Cultured COS7 cells were maintained at 37°C with 5% CO_2. The cell line was not further authenticated. Cells were tested negative for mycoplasma contamination by cytoplasmic DAPI staining.

METHOD DETAILS

Constructs and Protein Purification

The coding sequence of the full-length MORN4 (Accession number: NP_932776.1) was PCR amplified from a mouse cDNA library. The coding sequence of Myo3a-MBD was PCR amplified from the full-length human Myo3a plasmid as previously described (Liu et al., 2016). Norpa CC-PBM was obtained as described earlier (Ye et al., 2018). These constructs were cloned into a modified pET32M.3C vector for protein expression in bacteria. All point mutations were created with the standard PCR-based mutagenesis method and confirmed by DNA sequencing. For heterologous cell expressions, the WT and MBD mutant full-length human Myo3a (lacking the kinase domain) were cloned into a modified EGFP vector and the full-length mouse MORN4 was cloned into a modified mCherry vector. All proteins were expressed in *Escherichia coli* BL21 (DE3) cells. The N-terminal Trx-His_6-tagged proteins were purified with a Ni^{2+} Sepharose™ 6 Fast Flow column followed by a step of Superdex-200 size-exclusion chromatography.

Analytical Gel Filtration Chromatography

Protein samples (typically 100 μl at a concentration of 50 μM, pre-equilibrated with the column buffer composed of 50 mM Tris-HCl (pH 7.8), 1 mM DTT, 1 mM EDTA, and 100 mM NaCl) were analyzed on an ÄKTA FPLC system with a Superose-12 10/300 GL column (GE Healthcare).

Isothermal Titration Calorimetry Assay

Isothermal titration calorimetry (ITC) measurements were carried out on a MicroCal iTC_{200} at 25°C. Titration buffer contained 50 mM Tris-HCl, pH 7.8, 1 mM DTT, 1 mM EDTA and 200 mM NaCl. Each titration point was performed by injecting a 2 μL aliquot of a protein sample from a syringe into a protein sample in the cell with a time interval of 120 seconds to ensure that the titration curve returned to the baseline. The titration data were analyzed by Origin7.0 (Microcal).

Crystallography

Crystals of the MORN4/Myo3a-MBD complex (both in 50 mM Tris-HCl, pH 7.8, 100 mM NaCl, 1 mM EDTA, 1 mM DTT buffer) were obtained by sitting drop vapor diffusion methods at 16°C. Crystals were grown in buffer containing 0.5 M ammonium sulfate, 1.0 M lithium sulfate and 0.1 M sodium citrate tribasic at pH 5.6. Iodine derivatives were prepared by soaking crystals in the crystallization solution containing additional 400 mM KI for 1-2 min. Crystals were soaked in crystallization solution containing 25% glycerol for cryoprotection before diffraction experiments. Diffraction data were collected at BL17U1 or BL19U1 beamlines of the Shanghai Synchrotron Radiation Facility at 100 K at the wavelengths of 0.979 Å and 1.5 Å for native crystals and iodine derivatives, respectively. Data were processed and scaled using HKL2000 or HKL3000 (Otwinowski and Minor, 1997).

Using the iodine derivative dataset, the single-wavelength anomalous dispersion phase determination and initial model building were carried out in Autosol (Adams et al., 2010). Further manual model adjustment and refinement against the native dataset were completed iteratively using COOT (Emsley et al., 2010) and PHENIX (Adams et al., 2010). The final model was validated by MolProbity (Chen et al., 2010). The final refinement statistics are summarized in Table 1. All structure figures were prepared by PyMOL (http://www.pymol.org). The structure factors and coordinates of the structure have been deposited at the Protein Data Bank under the accession code of 6JLE.

Circular Dichroism Spectroscopy Based Thermal Denaturation

Thermal denaturation experiments of MORN4 WT and E63L were performed on a Chirascan CD spectrometer (Applied Photophysics) from 14°C to 60°C at a 2°C stepped temperature ramping. In both denaturation experiments, the ellipticity values at 215 nm were plotted as a function of temperature to obtain their denaturation profiles. The melting temperatures were calculated by fitting the curves using the sigmoid function.

Liposome-Binding Assay

Brain lipid extracts (Folch fraction I, Sigma B1502) were resuspended at 5 mg/ml in a buffer containing 50 mM Tris-HCl, pH 7.8, 100 mM NaCl, and 1 mM DTT by sonication (typically 10 cycles in ice-bath). The protein sample (5 μM) was incubated with 0.5 mg/ml liposomes in 50 μL of buffer for 15 min at room temperature and then spun at 200,000 g for 20 min at 4°C in a Beckman TLA100.1 rotor. The supernatants were removed for determination of proteins that did not bind to liposomes. The pellets were washed twice with the same buffer and brought to the same volume as the supernatant. The supernatant and the pellet proteins were subjected to SDS-PAGE and visualized by Coomassie blue staining.

COS7 Cell Culture, Transfection and Imaging

COS7 cells were cultured and transfected as described previously (Raval et al., 2016). Briefly, COS7 cells were cultured in DMEM (Invitrogen) supplemented with 4 mM L-glutamine, 1 mM Sodium Pyruvate, 4.5 g/L D-Glucose, 10% fetal bovine serum, and 100 units of penicillin-streptomycin. For transfections, ~35000-40000 COS7 cells were plated on acid washed 22 mm square glass coverslips

and allowed to adhere overnight. Cells were transfected with FUGENE HD transfection reagent (Promega) and imaged after ~20-30 hours. For transient transfection, 400 ng of the GFP-Myo3 plasmids and/or 100 ng of mCherry-MORN4 plasmid were used. For live-cell imaging, coverslips were placed in Rose chambers filled with Opti-MEM (without phenol red) supplemented with 5% fetal bovine serum and Penicillin-streptomycin. Nikon TE2000-PFS fluorescence microscope with a 60x/1.4 N.A. phase objective was used to acquire images. Images acquired from live-cell imaging were used for quantification of tip/cell body ratio and filopodial length. NIS-Elements AR (Nikon) and ImageJ were used to analysis and quantification.

QUANTIFICATION AND STATISTICAL ANALYSIS

Data of the tip to cell body ratios of GFP-Myo3aΔK (or its mutants) and mCherry-MORN4 when expressed in COS7 cells were expressed as mean ± SEM. At least 30 cells were quantified for each group from three or more batches of experiments. Experiments were not performed in a blinded fashion. The statistical analysis was performed using two-tailed independent sample T test in the Excel software; n.s, not significant (with p value >0.05), *p<0.05, **p<0.01, ***p<0.001. No data were excluded for analysis.

DATA AND CODE AVAILABILITY

Data Resources

The atomic coordinates of MORN4/Myo3a MBD complex have been deposited to the Protein Data Bank under accession code PDB: 6JLE.

Structure, Volume *27*

Supplemental Information

Structure of the MORN4/Myo3a Tail Complex Reveals MORN Repeats as Protein Binding Modules

Jianchao Li, Haiyang Liu, Manmeet H. Raval, Jun Wan, Christopher M. Yengo, Wei Liu, and Mingjie Zhang

Figure S1

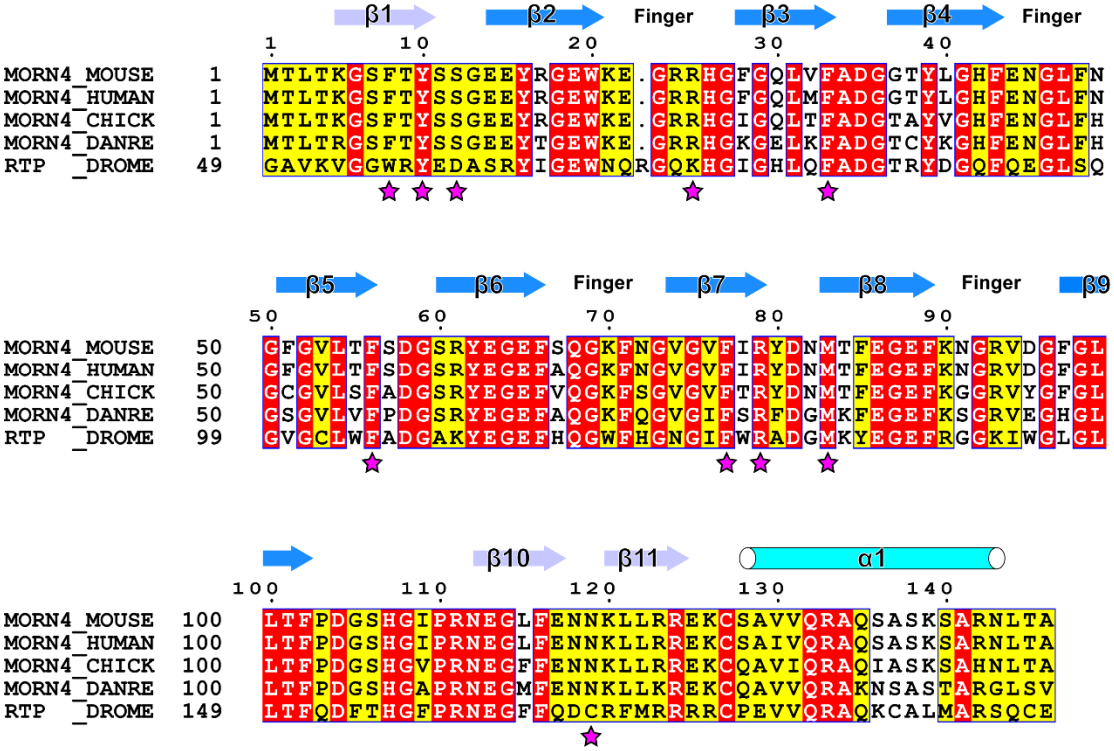

Figure S1: Sequence alignment of vertebrates MORN4 and *Drosophila* RTP, related to Figure 2 and Figure 3.

Residues that are identical and highly similar are indicated in red and yellow boxes, respectively. Residues critical for binding to Myo3a-MBD were highlighted by magenta stars.

Figure S2

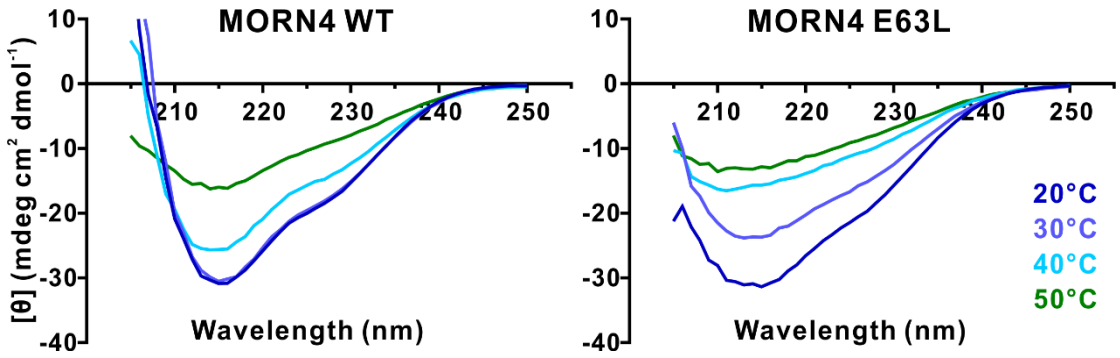

Fig. S2: The C-helix is important for MORN4 stability and binding to Myo3a-MBD, related to Figure 2.

Representative CD spectra of MORN4 WT (*left*) and E63L (*right*) at different temperatures.

Figure S3

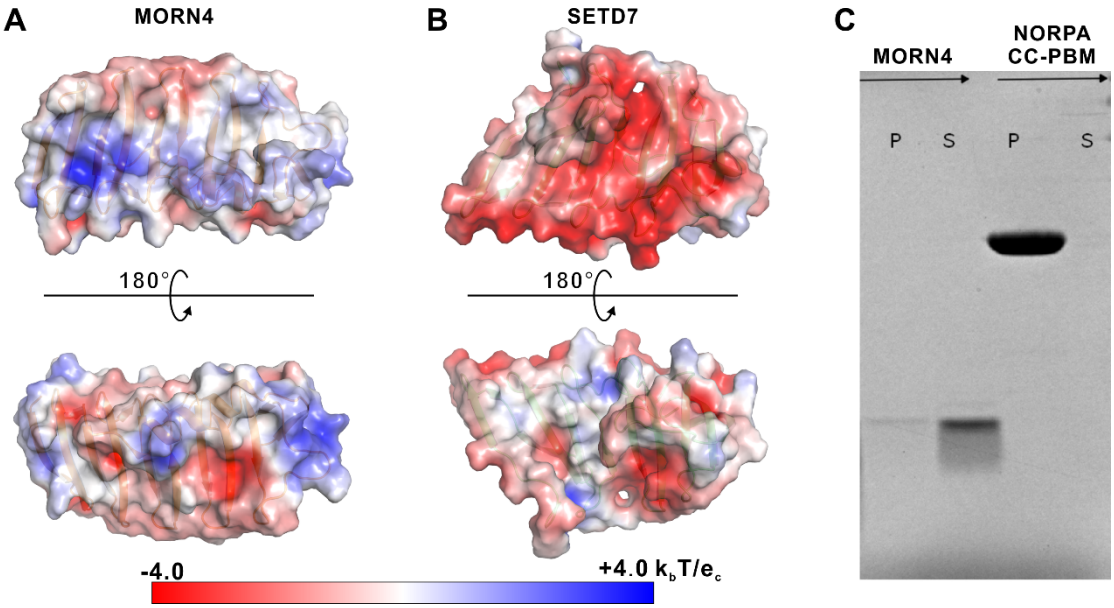

Fig. S3: MORN4 cannot bind to liposomes, related to Figure 4.

(A&B) Surface electrostatic potentials of MORN4 (A) and SETD7 (B) MORN repeats showing that no obvious positively charged surface exists for binding to negatively charged phospholipid membranes.

(C) Lipid sedimentation assay showing MORN4 cannot bind to liposomes. Fractions labeled 'S' and 'P' represent proteins that were recovered from the supernatants and pellets after centrifugation, denoting lipid-free and lipid-bound forms of the proteins, respectively. NORPA CC-PBM (aa 863-1095) was used as the positive control for lipid membrane binding (Ye et al., 2018).